JOURNAL OF MATERIALS SCIENCE 23 (1988) 217–222

Microstructure and magnetic properties of the permanent magnet material FeAlC

S. F. H. PARKER, P. J. GRUNDY, G. A. JONES
Department of Pure and Applied Physics, University of Salford, Salford M5 4WT, UK

I. BRIGGS, A. G. CLEGG
Magnet Centre, Physics Division, Priestman Building, Sunderland Polytechnic, Sunderland SR2 7EE, UK

The relationship between microstructure and magnetic properties of a series of permanent magnets based on the composition $Fe_{90}Al_8C_2$ (wt%) has been studied using X-ray diffractometry and transmission electron microscopy. We have used various fabrication methods, heat treatments and alloying elements in order to optimize the magnetic properties of these alloys and the properties obtained were found to compare favourably with commercially available cobalt steels.

1. Introduction

One of the earliest investigations of the FeAlC system was made by Morral [1] who looked at the iron-rich corner of the phase diagram. He found that alloys quenched from 1000° C consisted of three phases; an α-iron solid solution, an austenite containing some aluminium and carbon and an ordered fcc phase of the perovskite type, Fe_3AlC, which was later named the K-carbide. Several compounds having the perovskite structure have been reported [2] to be ferromagnetic, e.g. Fe_3PtN, Fe_3NiN, Mn_3AlC, and this was a possibility in the case of Fe_3AlC. In these compounds the carbon or nitrogen atoms occupy the body-centred site. In general, the K-carbide is non-stoichiometric and its lattice parameter can vary from 0.372 to 0.378 nm with increasing carbon concentration [3]. Our investigations have shown that the K-carbide is not ferromagnetic.

In our investigations we have been mainly concerned with alloy compositions and heat treatments which produce a large fraction of the K-carbide. We have succeeded in establishing what is probably the source of the limited magnetic hardness in these alloys. The inter-relationship of the austenite/ferrite/K-carbide phases will be described in terms of the scale of microstructure, crystallographic orientation and magnetic domain structure. The limitations presented by the relatively unfavourable microstructure of extruded alloys will be highlighted. The results of measurements of the stability of FeAlC magnets are also presented. These include estimates of flux losses, both reversible and irreversible and the resistance of the material to mechanical shock and contact losses.

2. Experimental details

The alloys investigated were based on the composition $FeAl_{7.8}C_{1.8}$ (wt %). Their chemical analysis is given in Table I. Specimens 1 and 5 were vacuum cast into ingots of 15 cm long and 1.25 cm diameter. Specimens 2 to 4 were vacuum cast into 10 cm diameter ingots and then extruded at 1200° C to form 1.9 cm diameter rods. Ingots were solution treated at 1200° C in an argon atmosphere and then quenched into either oil or polymer/water baths. Samples were heat treated at 350° C for various times to optimize their magnetic properties. Measurements of saturation magnetization against temperature were performed using a Sucksmith electronic ring balance.

Specimens for transmission electron microscopy were prepared by electropolishing using a 10% perchloric/90% glacial acetic acid electrolyte followed by ion thinning using 5 keV argon ions. The electron microscopes used in this investigation were a Jeol 200CX operating at 200 kV and an EM7 operating at 1 MV. Stability measurements were made on magnets of different length to diameter (L/D) ratios using an integrating fluxmeter [4].

3. Results and discussion

3.1. Magnetic properties

3.1.1. Vacuum-cast $FeAl_{7.74}C_{1.77}$ alloy

The effect of quench rate on the remanent magnetization

TABLE I Chemical analysis of alloys (wt %)

Specimen	Iron	Aluminium	Carbon	Boron	Tungsten	Molybdenum
1	90.49	7.74	1.77	–	–	–
2	90.67	7.54	1.79	–	–	–
3	90.17	7.53	1.81	–	0.49	–
4	90.32	7.34	1.82	–	–	0.52
5	89.54	7.51	1.80	1.15	–	–

0022–2461/88 $03.00 + .12

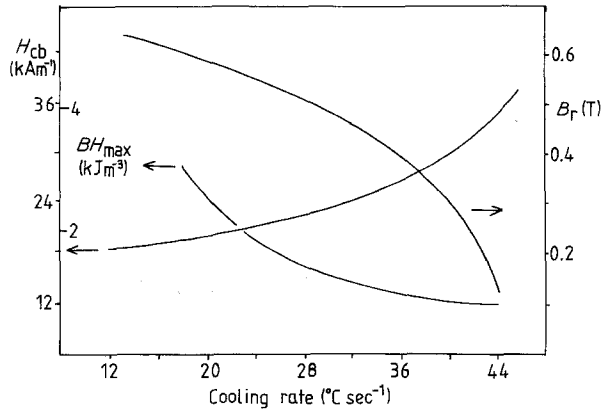

Figure 1 The variation of B_r, H_{cb} and BH_{max} with cooling rate for an FeAlC specimen.

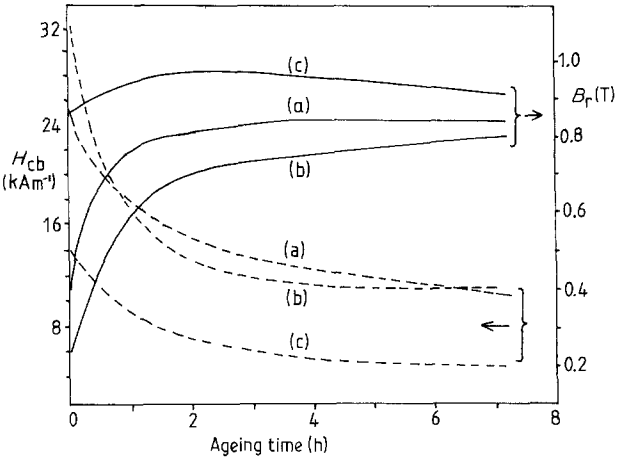

Figure 2 The variation in B_r and H_{cb} with ageing time at 350° C: (a) oil quenched, (b) 44° C sec^{-1}, (c) 16° C sec^{-1}.

(B_r), coercivity (H_{cb}) and energy product (BH_{max}) can be seen in Fig. 1. The water-quenched sample which has the fastest quench rate of 30° C sec^{-1} has the lowest value of B_r and the highest coercivity. Reducing the quench rate results in an increase in B_r at the expense of coercivity. A similar effect is observed during heat treatment at 350° C. The variation of B_r and H_{cb} with annealing time is shown in Fig. 2 for various cooling rates. The highest value of BH_{max} obtained was 5.68 kJ m^{-3} for an oil-quenched specimen aged for 3 h at 350° C. The variation of saturation magnetization with temperature is shown in Fig. 3 for an oil-quenched specimen after various heat treatments. This shows a transformation taking place at around 300° C which produces a ferromagnetic phase. On cooling, the magnetization follows a simple curve indicating the presence of a single ferromagnetic phase.

3.1.2. Quaternary alloys

In an attempt to improve the magnetic properties of the ternary alloy, additions of tungsten, molybdenum and boron were made. Two of these alloys were extruded in a 5 : 1 reduction from 1200° C to see if this would introduce anisotropy along the length of the rod. The boron-containing alloy was found to be very brittle and we were unable to extrude a rod from it. The magnetic properties of the alloys are summarized in Table II. The as-extruded alloys have a relatively low coercivity, the highest value obtained was 6 kA m^{-1} for the molybdenum-containing alloy. This result was not surprising because the alloys were essentially air cooled and slow cooling rates tend to produce low coercivities in these materials. A significant improvement in BH_{max} was observed after oil quenching from 1200° C. The tungsten-containing alloy gave the highest coercivity and energy product of 20.2 kA m^{-1} and 3.2 kJ m^{-3}, respectively. Subsequent heat treatment at 350° C produced a further improvement in magnetic properties. In the case of the tungsten- and molybdenum-containing alloys changes in B_r and H_c during ageing followed the same trend as observed in the ternary alloy, with an increase in B_r at the expense of coercivity. In contrast, ageing of the boron-containing alloy resulted in an increase in both B_r and H_c. The highest energy product obtained was 4.08 kJ m^{-3} for the tungsten-containing alloy. In general, the addition of molybdenum or tungsten to the ternary alloy led to an increase in coercivity and a fall in remanent magnetization. There is also a marginal improvement in BH_{max} of around 2%.

3.2. X-ray diffractometry

An X-ray diffractometry trace taken from the polished

TABLE II A comparison of the magnetic properties of FeAlC-based alloys

Composition	Heat treatment	M_s (mT)	B_r (mT)	H_c (kA m^{-1})	BH_{max} (kJ m^{-3})
FeAlC	as-extruded	1089	596	3.84	0.72
	oil quench (1200° C) + 2 h at 350° C	1041	753	10.96	4.00
FeAlCW	as-extruded	1039	583	4.82	0.88
	oil quench (1200° C) + 2 h at 350° C	1004	720	11.84	4.08
FeAlCMo	as-extruded	994	558	6.01	1.12
	oil quench (1200° C) + 2 h at 350° C	1004	715	11.20	4.00
FeAlCB	as-cast	922	278	2.40	0.24
	oil-quench (1200° C) + 3 h at 350° C	932	448	7.20	0.81

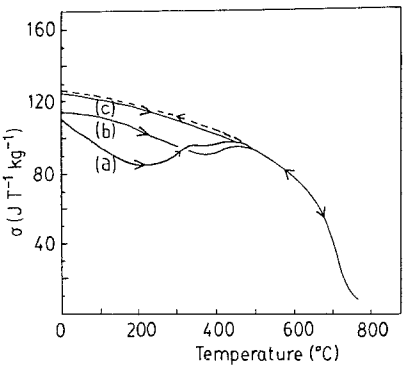

Figure 3 Saturation magnetization against temperature for an FeAlC alloy oil quenched from 1200° C: (a) as-quenched, (b) 45 min, (c) 3 h at 350° C.

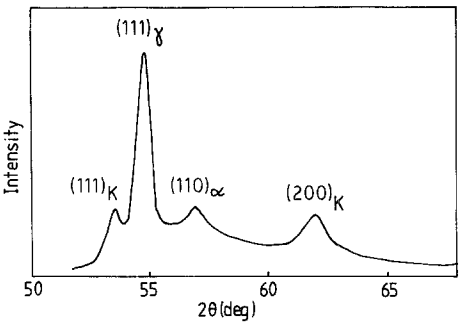

Figure 4 X-ray diffractometer trace taken from a water-quenched sample of FeAlC.

surface of a water-quenched specimen of $FeAl_{7.74}C_{1.77}$ using Fe$K\alpha$ radiation can be seen in Fig. 4. The peaks centred at 54° can be identified as the (1 1 1) reflections of the austenite (γ) and perovskite (K) phases, the greater intensity peak being that of austenite. The peak centred at 57° is the (1 1 0) reflection of the bcc ferrite (α) phase. Traces taken from oil-quenched specimens showed a reduction in the amount of retained austenite. Heat treatment led to the disappearance of the austenite peaks and a growth in the ferrite and perovskite peaks. It is therefore concluded that the transformation of austenite into ferrite and perovskite is responsible for the changes observed in the magnetization curves (Fig. 3) and for the increase in B_r and saturation magnetization observed during heat treatment.

The trace obtained using Mo$K\alpha$ radiation from an oil-quenched (1200° C) and heat-treated specimen of $FeAl_{7.51}C_{1.8}B_{1.15}$ is shown in Fig. 5. Four main phases can be identified; a bcc ferrite (a_0 = 0.287 nm), an ordered fcc perovskite phase (a_0 = 0.375 nm), an fcc $Fe_{23}(B, C)_6$ phase (a_0 = 1.062 nm) and an orthorhombic $Fe_3(B, C)$ phase (a_0 = 0.445 nm, b_0 = 0.543 nm, c_0 = 0.666 nm). The ferrite and perovskite phases were also observed in the ternary FeAlC alloy along with a small amount of Fe_3C cementite identified by electron diffraction. However, the orthorhombic $Fe_3(B, C)$ phase found in this alloy has a lattice constant closer to that of Fe_3B. The difference in magnetic properties between the FeAlCB alloy and the FeAlC alloy is undoubtedly due to the presence of the additional boride phases.

Measurements made by Nicholson [5] on the orthorhombic $Fe_3(B, C)$ phase showed an increase in both saturation magnetization and Curie temperature when boron was added to the binary Fe_3C cementite phase. In addition, the Fe_3C phase has a uniaxial anisotropy along the c-axis with an anisotropy constant comparable with that of cobalt. If the $Fe_3(B, C)$ phase has a similar anisotropy constant combined with its high Curie temperature and saturation magnetization, then it should improve the magnetic properties of the ternary alloy provided it can be incorporated into the same Widmanstatten type microstructure of thin plates of ferromagnetic material in a non-ferromagnetic matrix.

3.3. Transmission electron microscopy

3.3.1. Vacuum-cast FeAlC alloy

In an earlier paper [6] we reported some TEM observations made on the ternary alloy which we have included here for completeness. A typical micrograph of an oil-quenched and heat-treated specimen of $FeAl_{7.74}C_{1.77}$ is shown in Fig. 6a. The micrograph was obtained using high-voltage electron microscopy and shows the uniformity of Widmanstatten-type ferrite precipitates within a perovskite matrix. The rectangular features are the Fe_3AlC perovskite phase. Fig. 6b shows the same region of the foil after tilting to bring into contrast fine Widmanstatten-type ferrite regions.

Specimens prepared from oil-quenched samples prior to heat treatment show a similar microstructure

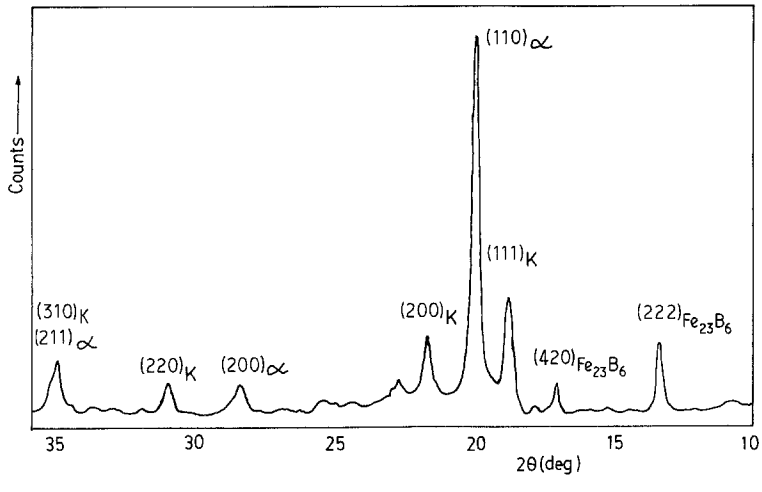

Figure 5 X-ray diffractometer trace taken from an oil-quenched sample of FeAlCB.

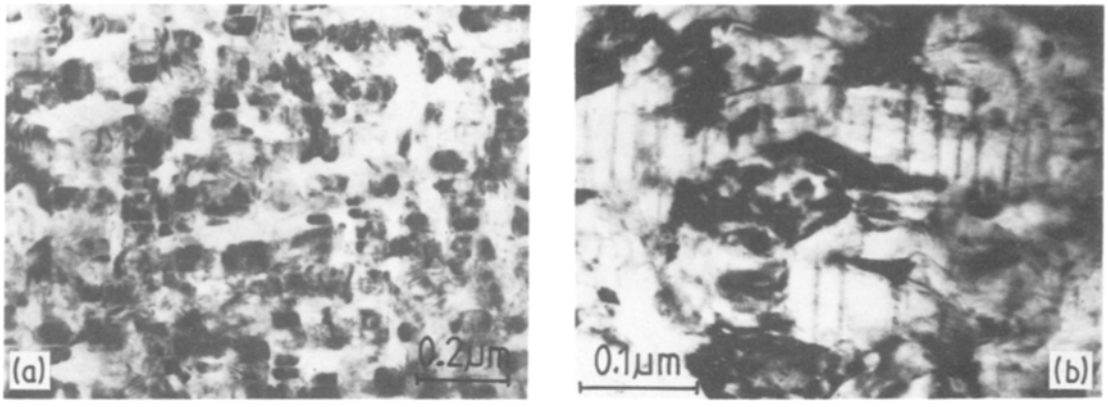

Figure 6 HVEM micrographs of an oil-quenched and heat-treated specimen of FeAlC.

except that in some regions there is a lamellar structure which can be seen in Fig. 7a. In addition electron diffraction patterns revealed extra spots from retained austenite. These spots were very close to those of the perovskite and a lattice parameter of 0.365 nm was determined for this phase. An electron diffraction pattern for an oil-quenched specimen is seen in Fig. 7b which shows single-crystal patterns for the austenite and perovskite phases. In contrast the ferrite spots, although associated with those of the austenite and perovskite, are smeared out over arcs. Analysis of such diffraction patterns and other composite patterns indicates definite orientation relationships between the three phases. Fig. 8 gives a schematic outline of the proposed relationship which is of the form

$$(1\,0\,0)_\gamma \parallel (1\,0\,0)_K \parallel (1\,0\,0)_\alpha \quad (1a)$$

$$[0\,1\,0]_\gamma \parallel [0\,1\,0]_K \parallel [0\,1\,1]_\alpha \quad (1b)$$

Naturally a good lattice fit is obtained between the two face-centred phases (γ, K) but a reasonable fit ($< 10\%$ mismatch) also exists between the (γ, K) and α phases. Nevertheless a mismatch of $\sim 10\%$ is likely to be accompanied by considerable lattice strain (revealed as ferrite arcs in Figs. 7b) and perhaps interfacial dislocations. In the fully transformed regions the carbide particles are therefore surrounded by a network of thin, interconnecting lamellae or plates of ferrite. This microstructure has important consequences for the domain structure and magnetic hardness of the material as discussed below. Incidentally it may be inferred from Equation 1 that for a carbide morphology based on cuboids, a single orientation of carbide may appear with up to three simultaneous equivalent orientations of ferrite corresponding to plates on pairs of opposite faces. Evidence for this is found in the electron diffraction patterns.

In addition to the three phases already identified, electron diffraction analysis of some samples revealed weak reflections from a fourth phase. These reflections became stronger in an oil-quenched specimen which had been annealed for 30 h at 350° C but were not sufficiently numerous to make a positive identification of the phase. However, the reflections did appear to fit those of the orthorhombic Fe_3C ($a_0 = 0.452$ nm, $b_0 = 0.509$ nm, $c_0 = 0.674$ nm) and this phase was positively identified in the extruded alloys as discussed below.

The finely divided microstructure of the material is reflected in the magnetic domain structure observed by Lorentz microscopy. Fig. 9 shows the complicated domain structure in an oil-quenched and heat-treated specimen which appears to be associated with the boundaries between the ferrite and K-carbide phases. The average domain size seen here is approximately 0.1 μm. In some regions, longer principal domain walls can be seen. In all cases the domain walls run along the direction of the ferrite plates which correspond to the [1 0 0] K direction. As the K-carbide is non-ferromagnetic, the direction of magnetization would tend to lie in the plane of the ferrite plates because of their shape anisotropy, and this is borne out by the domain structure observed.

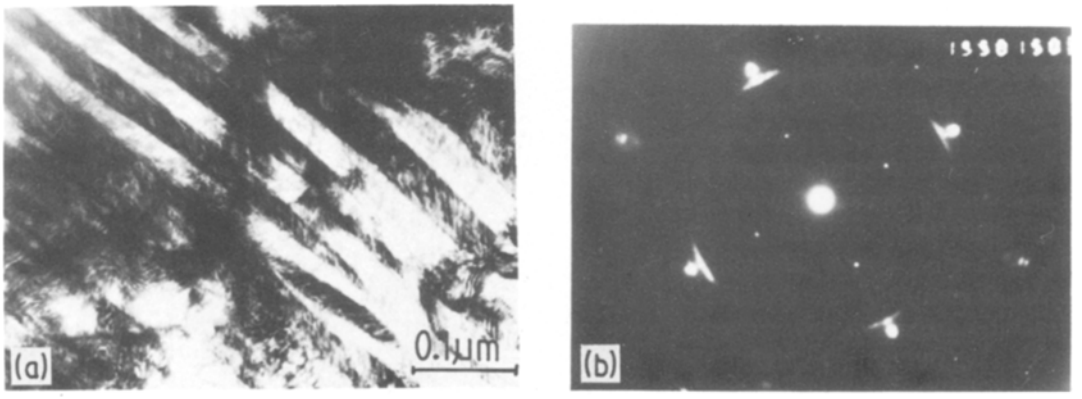

Figure 7 Electron micrograph and diffraction pattern of an oil-quenched specimen of FeAlC.

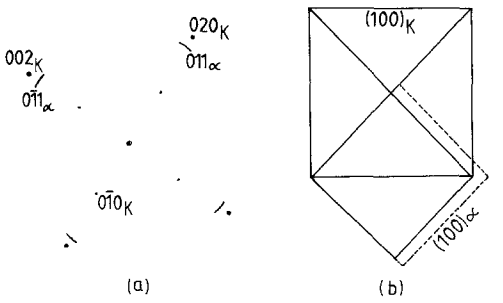

Figure 8 Orientation relationship between ferrite and perovskite phases: (a) diffraction pattern, (b) lattice fit.

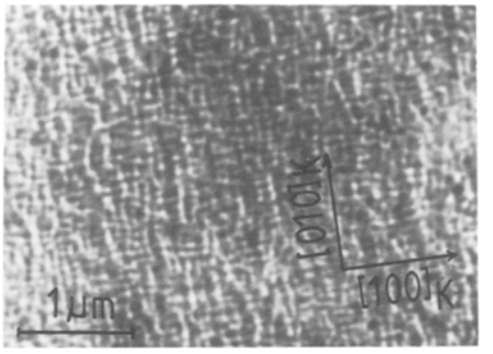

Figure 9 Lorentz electron micrograph of an oil-quenched and aged specimen of FeAlC.

3.3.2. Quaternary alloys

The microstructure observed in the as-extruded ternary and the molybdenum- and tungsten-containing quaternary alloys can be seen in Fig. 10. In some regions, Fig. 10a, the microstructure is similar to that observed in the oil-quenched specimens discussed earlier. In other regions, Fig. 10b, the microstructure is on a larger scale with the boundaries between phases being more rounded. Some regions, Fig. 10c, show spherulites of perovskite within grains of ferrite. Here the ferrite regions contain a fine dispersion of Fe_3C cementite. The microstructure was similar for the as-extruded ternary and the molybdenum- and tungsten-containing quaternary alloys, except that the fine Widmanstatten-type structure was more common in the molybdenum-containing alloy and least common in the ternary alloy. It would therefore appear that air cooling is not sufficiently fast to form the fine Widmanstatten-type structure necessary to produce high coercivities. After oil quenching, all three alloys developed the finely divided microstructure observed in the vacuum-cast ternary alloy with a subsequent improvement in magnetic properties. Incidentally, we were unable to detect the presence of carbides of molybdenum or tungsten probably because of the relatively low heat-treatment temperatures. Increasing the ageing temperature may have resulted in the precipitation of these carbides but would have destroyed the fine microstructure.

The variation in microstructure within an oil-quenched (1200° C) and heat-treated specimen of $FeAl_{7.51}C_{1.8}B_{1.15}$ can be seen in Fig. 11. The majority of the specimen consists of regions such as those seen in Fig. 6a consisting of Widmanstatten-type ferrite precipitates within a perovskite matrix. This is the type of microstructure found throughout the oil-quenched FeAlC alloy and is responsible for the increase in coercivity after quenching. Other regions, Fig. 11a, consist of ferrite grains containing finely dispersed cementite particles and larger Fe_3AlC grains. This type of structure was also found in the as-extruded alloys and in the ternary alloy after slow cooling from the austenitic phase. This structure when present throughout the alloy results in low coercivities. A third region observed in the boron-containing alloy, Fig. 11b, consists of an $Fe_{23}(B, C)_6$ matrix containing spherulites of Fe_3AlC. The $Fe_{23}(B, C)_6$ boride phase has an fcc structure with a lattice constant of $a_0 = 1.062$ nm.

It would therefore appear that the addition of boron to the ternary alloy suppresses the formation of the fine Widmanstatten-type microstructure which is necessary to produce a high coercivity. X-ray diffractometry revealed the presence of small amounts of the ferromagnetic $Fe_3(B, C)$ phase which has a higher Curie point than the binary Fe_3C cementite phase and could improve the magnetic properties of the ternary

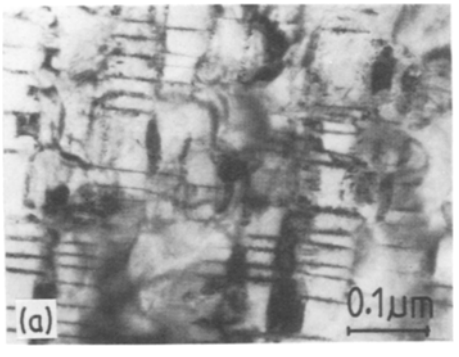

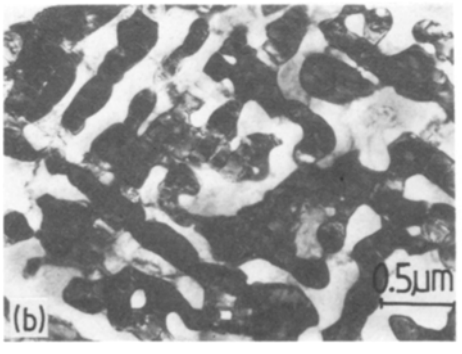

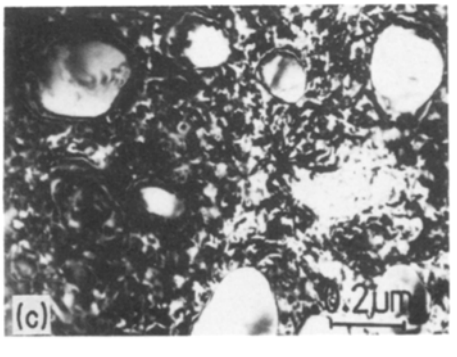

Figure 10 Electron micrographs of as-extruded specimens of (a, b) FeAlCMo, (c) FeAlCW.

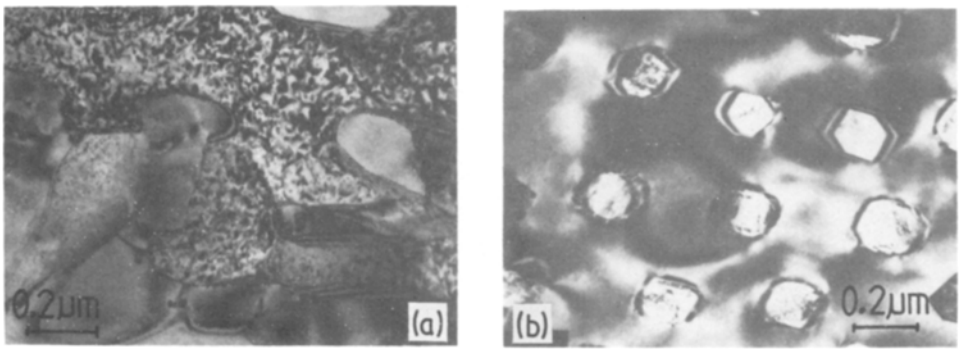

Figure 11 Transmission electron micrographs of an aged specimen of FeAlCB.

FeAlC alloy by introducing some magneto-crystalline anisotropy.

3.4. Stability measurements

The stability of an oil-quenched (1200° C) and heat-treated FeAlC magnet to temperature, mechanical shock and contact losses is summarized in Table III for a rod of length to diameter ratio $L/D = 5$. The mechanical shock tests were performed by dropping the magnet from a height of 1 m on to a wooden block. Contact losses vary greatly depending on how the tests are carried out, the procedure we used was designed to give the largest flux losses. The procedure involved bringing the side of the bar into contact with a mild steel block and then sliding the bar off the block in a direction parallel to its direction of magnetization. Examination of Table III shows that FeAlC compares favourably with other commercially available steels.

4. Conclusion

Magnetic measurements on the ternary FeAlC alloy indicate the presence of a single ferromagnetic phase, i.e. the bcc ferrite phase. Lorentz microscopy of slowly cooled and extruded alloys where fairly large grains of Fe_3AlC can be found did not show the presence of domain walls. These observations lead to the conclusion that the Fe_3AlC perovskite phase is not ferromagnetic. The type of microstructure which produces the highest coercivities in these alloys consists of fine Widmanstatten-type ferrite precipitates in a non-magnetic perovskite matrix.

In our attempts to improve the magnetic properties of the ternary alloy, additions of molybdenum, tungsten and boron were made. The addition of boron to the ternary alloy introduced an anisotropic $Fe_3(B, C)$ phase and if the preferred fine microstructure could be retained in FeAlCB, significant improvements are possible. Our extrusion experiments produced inferior properties. This was clearly associated with the coarse microstructure obtained. Larger reduction factors and faster cooling after reduction could give improvements here. A comparison of FeAlC with other commercially available steels makes it an excellent substitute for cobalt steel magnets. Values of BH_{max}, other extrinsic magnetic properties and the stability of the material (particularly to temperature, contact and impact) makes it an excellent choice for applications such as long bars and in cheap motors and pumps.

TABLE III A comparison of the stability of FeAlC with other commercially available steels ($L/D = 5$)

Material	% Loss of open circuit flux			
	1000 h at 20° C	After heating to 300° C	10 Contacts with mild steel block	200 Impacts
Carbon steel	4.89	65.2	10.5	5.86
9% Cobalt	2.14	15.6	17.4	2.58
15% Cobalt	1.64	19.9	20.8	3.19
35% Cobalt	0.80	11.2	11.5	4.90
FeAlC	1.68	17.4	6.60	1.55

Acknowledgement

This work was supported by the EEC Materials Substitution Programme (contract no. SUM-032-UK).

References

1. F. R. MORRAL, *J. Iron Steel Inst.* **130** (1934) 419.
2. R. OSHIMA and C. M. WAYMAN, *Trans. Jpn Inst. Metals* **16** (1975) 111.
3. P. J. JAMES, *J. Iron Steel Inst.* **207** (1969) 54.
4. I. BRIGGS and A. CLEGG, *IEEE Trans Magn.* **MAG-20** (1984) 1628.
5. M. E. NICHOLSON, *J. Metals* January (1975) 1.
6. S. F. H. PARKER, P. J. GRUNDY and G. A. JONES, *IEEE Trans Magn.* **Mag-20** (1984) 1630.

Received 11 February
and accepted 29 April 1987